Journal of Alloys and Compounds, 186 (1992) 153–160
JALCOM 266

Band structure influence on cohesion in quasi-crystals

P. M. Ossi
Dipartimento di Ingegneria Nucleare, Politecnico di Milano, Via Ponzio 34/3, 20133 Milano (Italy)
and Unità cINFM di Trento, 38050 Povo (TN) (Italy)

(Received February 1, 1992)

Abstract

The nearly free electron model has been applied to investigate the origin of structural stability in quasi-crystalline alloys containing s, p and d elements, through an analysis of X-ray or neutron diffraction patterns. The existence of a Hume-Rothery relation and the presence of a pseudogap in the density of states near the Fermi level is discussed making reference to recent measurements of electronic properties of quasi-crystals. On the basis of the agreement between model predictions and experimental data, a specific electron phase, associated with the quasi-crystalline state, is defined.

1. Introduction

Soon after quasi-crystals (QCs) were discovered, it was proposed that an electronic mechanism, possibly of the Hume-Rothery–Jones (HRJ) type, was responsible for the cohesion of this class of solids [1].

The hypothesis is supported by the unique features of QC diffraction patterns [2], which exhibit fivefold orientational symmetry, rigidly forbidden by classical crystallography, as well as being a sum of δ functions, distributed in a dense way.

Such an anomaly means that electrons in QCs are scattered strongly and everywhere; also, the very high electrical resistivity measured in stable QCs, with a low degree of microstructural and phason disorder [3], indicates a strong electron–lattice interaction, which in turn can imply that the cohesion mechanism is of an electronic nature.

In the case of crystalline materials, the most popular case of band structure influence on structural stability is provided by the electron phases, for which Hume-Rothery proposed that with different structures were associated boundary values of the average number $\langle Z \rangle$ of electrons per atom [4]. Jones gave a nearly free electron (NFE) picture of the Fermi surface (FS)–Brillouin zone (BZ) contact which explains the Hume-Rothery phase boundaries [5]. At

$$\bar{\mathbf{Q}} = 2\bar{\mathbf{k}}_F \tag{1}$$

with $\bar{\mathbf{Q}}$ a reciprocal lattice vector and $\bar{\mathbf{k}}_F$ the Fermi wavevector, a gap opens in the dispersion relation $E(\bar{\mathbf{k}})$, leading to an energy lowering of occupied

0925-8388/92/$5.00

states and to an energy increase of empty states, with the Fermi level E_F lying in the gap. The net result is an enhancement of the cohesion energy of the system.

An analogous mechanism was proposed to explain the stability of amorphous alloys [6] and the pseudogap existence was proved in illustrative examples [7].

In this work the idea that the quasi-crystalline state can be associated with a specific electron phase is put forward, starting from an analysis of the diffraction behaviour of several spd QCs, in the framework of the NFE approximation.

2. Model and results

In QCs, as in their crystalline approximants, the strongest diffraction peaks are situated in the neighbourhood of $\bar{\mathbf{Q}} = 30$ nm^{-1}; in the crystalline case, such peaks invariably satisfy eqn. (1), and a gap at E_F is observed. Is the same equation obeyed also by QCs and does a pseudogap exist, *i.e.* is there evidence for a minimum in the electronic density of states (DOS) at E_F?

Indeed, if a QC satisfied a relation of the HRJ type, the high multiplicity of the relevant diffraction peaks, which implies a nearly spherical pseudo-BZ, would lead to an enhanced stabilizing effect, as all states for which

$$|\bar{\mathbf{k}}| = \bar{\mathbf{Q}}/2 \tag{2}$$

should be affected.

We consider a set of 15 spd QCs, formed from an s (lithium, sodium, magnesium), a p (aluminium, gallium, germanium, tin) and a near-noble d (nickel, palladium, platinum, zinc, copper, silver, gold) component, for which experimental X-ray or neutron diffraction patterns are available in the literature, in the form either of a diffractogram or of tabulation. We extract experimental $\bar{\mathbf{k}}_F$ values from the data, through

$$\bar{\mathbf{k}}_{F,exp} = \bar{\mathbf{Q}}_{exp}/2 \tag{3}$$

where the $\bar{\mathbf{Q}}_{exp}$ value is that of the most intense diffraction peak. For a comparison we also consider prototype Al–Si–TM (TM ≡ transition metal) ternary and quaternary alloys, the systems $Ti_{56}Ni_{28}Si_{16}$ [8] and $Ti_{56}Ni_{25.5}Fe_{2.5}Si_{16}$ [9], involving only TMs, apart from stabilizing silicon, and the two stable QCs $Al_{65}Cu_{20}Fe_{15}$ [10] and $Al_{65}Cu_{15}Co_{20}$ [11], giving a total of 23 compounds. For spd QCs, the considered diffraction peak is (222100), with multiplicity $m = 30$, while for Al–TM systems we take the (211111) ($m = 12$) or the (221001) ($m = 30$) peak. Based on the criterion of choosing the most intense diffraction peak, our choice reflects the qualitative difference between the diffraction patterns of the two families of quasi-crystalline compounds; the (222100) peak is nearly absent in Al–TM systems, while the (211111) and (221001) peaks are extremely weak in spd alloys.

For all systems, values of $\bar{\mathbf{k}}_{F,NFE}$ are calculated in the framework of an NFE model. For a spherical FS and assuming a spherical pseudo-BZ,

$$\frac{4}{3}\pi\bar{\mathbf{k}}_{F,NFE} = \frac{(2\pi)^3/2\langle Z\rangle}{(4/3)\,\pi\langle\bar{r}\rangle^3\eta} \tag{4}$$

The volume of the FS equals the ratio between the volumes of the occupied electron states and of the pseudo-BZ.

Here, considering an $A_{1-x-y}B_xC_y$ alloy, $\langle\bar{r}\rangle$ is the average alloy atomic radius:

$$\langle\bar{r}\rangle = r_A(1-x-y) + r_B x + r_C y \tag{5a}$$

is the packing efficiency, assumed to be 0.688 for icosahedral packing [12] and the average number of electrons per atom of the alloy is given by

$$\langle Z\rangle = Z_A(1-x-y) \pm Z_B x \pm Z_C y \tag{5b}$$

The minus sign in eqn. (5b) means that when TMs are involved a charge transfer to their d bands is assumed; the effect is indeed observed [13] and it is attributed to compensation of the unpaired spins of d electrons. While TMs are usually assigned 0 valency when $\langle Z\rangle$ is calculated for crystalline electron compounds we refer to a phenomenological model of TMs [14] and to X-ray studies on Al–TM alloys [15] for manganese and chromium valencies, while the values for iron, cobalt and nickel are taken from an NFE study of the structural properties of glassy TM–polyvalent element alloys [16]. In the cases of inter-TM alloys, charge transfer from the early TM titanium to the late TMs nickel and iron is considered on the basis of Pauling's electronegativities, and a valency +2 is assigned to titanium [17]. In Table 1 are listed atomic radii and valencies used in our analysis.

Table 2 provides alloy compositions, $\bar{\mathbf{k}}_{F,exp}$ values and calculated average electron per atom ratios $\langle Z\rangle$; the index of each alloy is used to identify data points in Fig. 1.

Figure 1 is a plot of $\bar{\mathbf{k}}_{F,NFE}$ values derived from eqn. (4) *vs.* $\bar{\mathbf{k}}_{F,exp}$ values. The full line gives the locus of "ideal" NFE systems; the broken line is the result of a least-squares fit on the data points. For the quite large group of representative alloys here considered, the agreement appears good.

3. Discussion

Examining Fig. 1, we do not observe a marked effect of the preparation technique used to produce quasi-crystalline samples on their properties. The behaviour of $Al_{65}Cu_{15}Co_{20}$ (index 19) and of $Al_{65}Cu_{20}Fe_{15}$ (index 21) stable QCs, which are comparatively defect free with respect to metastable QCs, does not seem to be qualitatively different from that of the other systems; this could simply imply that the NFE picture is intrinsically too coarse to take into account finer details of alloy scattering behaviour.

Icosahedral and decagonal phases fit equally well in the NFE scheme; in fact, in alloys exhibiting coexistence of both types of incommensurate

TABLE 1

Valencies and atomic radii for the constituents of the studied quasi-crystals

Element	Valency	Atomic radius (nm)
Al	+3	0.143
Ga	+3	0.125
Ge	+4	0.122
Li	+1	0.152
Mg	+2	0.160
Si	+4	0.117
Pd	−2	0.137
Pt	−4	0.138
Zn	+2	0.133
Cu	+1	0.128
Ag	+1	0.145
Au	+1	0.144
Ti	+2	0.146
Mn	−3.66	0.125
Cr	−4.66	0.129
Fe	−1.11	0.126
Co	−1.03	0.125
Ni	−1.14	0.124

Negative valencies imply charge transfer to TM d bands (see text).

structures, contributions to the diffraction pattern by the different phases cannot be distinguished within experimental uncertainty [25].

Various parameters have been used to interpret icosahedral phase occurrence and stability; while the promising atomic size factor was recently found to fail [26], the average conduction electron density $\langle Z \rangle$ appears significant. The spd QCs so far obtained fall in the limited $\langle Z \rangle$ range 2.1–2.6; if Al–TM QCs are also considered, the lower $\langle Z \rangle$ limit extends down to about 1.44, in agreement with our previous analysis [27].

The validity of the NFE picture to describe the electronic behaviour of QCs lends support to the idea that a pseudogap at E_F is present in materials with such a structure. Apart from the exception of $Mg_{32}Zn_{52}Ga_{16}$, for which the measured electronic specific heat coefficient γ was as low as 0.18 mJ mol^{-1} K^{-2} [28], in general γ does not appreciably change in spd alloys, either in crystalline or in quasi-crystalline phases [29].

When plotted against the electron concentration $\langle Z \rangle$, γ exhibits a universal trend, independent of alloy system, and it decreases with decreasing $\langle Z \rangle$ from the free electron value, down to about one-third of the free electron value. Alloys having relatively low values of the electrical resistivity ρ, lower than say 100 $\mu\Omega$ cm, exhibit essentially free-electron-like γ values, while a decrease in γ coincides with a sharp rise in ρ.

The temperature dependence of the electrical resistivity ρ in spd alloys was found to exhibit trends analogous to those exhibited by non-magnetic amorphous alloys [30]. The typology of the ρ–T curves can be interpreted

TABLE 2

Experimental values of the Fermi wavenumber $\bar{k}_{F,exp}$ together with the main diffraction peaks from which they have been extracted, and calculated average electron concentrations $\langle Z \rangle$ per atom for the quasi-crystals listed in the first column

Alloy	Index	$\bar{k}_{F,exp}$ (nm^{-1})	Diffraction peak (X-rays)	Reference	$\langle Z \rangle$
$Al_{85}Mn_{14}Si$	1	15.19^{N}	(110000)	18	2.078
$Ga_{16}Mg_{32}Zn_{52}$	2	15.59	(222100)	19	2.160
$Al_{25}Mg_{37.5}Zn_{37.5}$	3	15.31	(222100)	19	2.250
$Al_{60}Si_{20}Cr_{20}$	4	15.21	(221001)	19	1.668
$Al_{74}Mn_{15}Si_{6}Fe_{5}$	5	15.40	(221001)	20	1.855
$Al_{55}Mg_{36}Cu_{9}$	6	15.30	(222100)	21	2.400
$Ga_{24}Mg_{36}Zn_{40}$	7	15.55	(222100)	22	1.600
$Al_{59}Li_{30}Cu_{11}$	8	15.85^{D}	(222100)	20	2.180
$Al_{60}Li_{30}Au_{10}$	9	15.70	(222100)	20	2.200
$Al_{50}Mg_{35}Ag_{15}$	10	15.23	(222100)	20	2.350
$Al_{51}Li_{32}Zn_{17}$	11	15.57	(222100)	20	2.190
$Al_{60}Mg_{38}Pd_{2}$	12	15.10	(222100)	23	2.556
$Al_{60}Mg_{38}Pt_{2}$	13	15.05	(222100)	23	2.480
$Al_{60}Mg_{38}Ag_{2}$	14	15.07	(222100)	23	2.540
$Al_{50}Mg_{48}Ni_{2}$	15	15.10	(222100)	23	2.435
$Al_{50}Mg_{48}Cu_{2}$	16	15.11	(222100)	23	2.480
$Al_{50}Mg_{48}Au_{2}$	17	15.06	(222100)	23	2.480
$Al_{85}Mn_{7}Cr_{8}$	18	15.07^{N}	(221001)	18	1.921
$Al_{65}Cu_{15}Co_{20}$	19	15.54^{D}	(000001)	11	2.044
$Al_{56.1}Li_{33.7}Cu_{10.2}$	20	15.74^{D}	(111101)	24	2.122
$Al_{65}Cu_{20}Fe_{15}$	21	15.71	(221001)	10	1.983
$Ti_{56}Ni_{28}Si_{16}$	22	14.52	(221001)	8	1.441
$Ti_{56}Ni_{25.5}Fe_{2.5}Si_{16}$	23	14.54	(221001)	9	1.442

The sample numbers in the second column are used to indicate data points in Fig. 1. N, neutron diffraction data; D, decagonal phase.

in terms of the generalized Faber–Ziman theory, based on the standard Boltzmann transport equation; however, while the theory predicts a decreasing ρ when the structure factor is sharpened, in $Mg_{39.5}Zn_{40}Ga_{20.5}$, which has no d states near E_F, an increase in ρ on heating is observed, while at the same time the diffraction peaks sharpen. A high ρ value was found in $Al_{55}Li_{35.8}Cu_{9.2}$ [31]; the ρ–T curve displays features typical of the breakdown of the standard Boltzmann scattering mechanism, occurring when the mean free path of conduction electrons is comparable with the average atomic distance, while at the same time the concentration of conducting electrons at E_F is consistently lowered, as experimentally observed.

A unique behaviour, with a minimum in the electrical resistivity *vs.* temperature characteristic, was reported for quasi-crystalline $Ti_{56}Ni_{28-x}Fe_xSi_{16}$ alloys [30]; the position of the minimum is sensitive to alloy composition c. In the framework of Faber–Ziman diffraction theory, the main contribution to ρ depends on structure [32]; in the case of TiNiFeSi QCs two competitive mechanisms are required to reproduce the observed ρ *vs.* T trend. From an

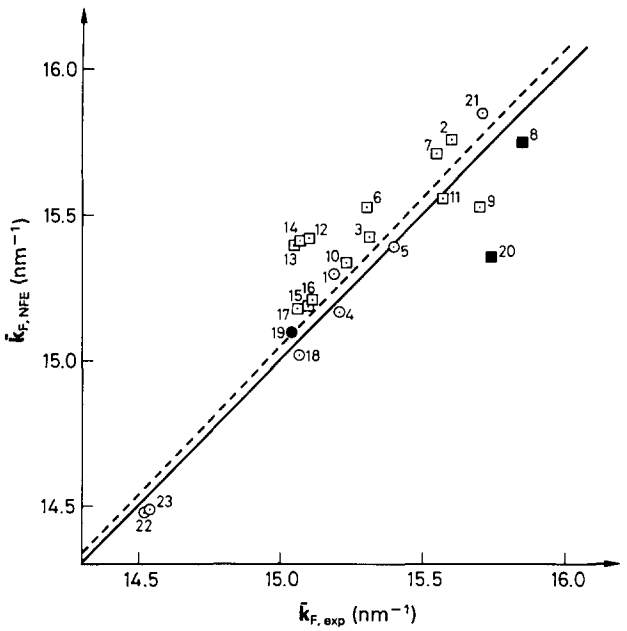

Fig. 1. Calculated Fermi wavenumbers $\bar{k}_{F,NFE}$ as obtained in an NFE scheme *vs.* experimental Fermi wavenumbers $\bar{k}_{F,exp}$. Data point numerals refer to the corresponding alloys listed in Table 2: ⊙, Al–TM QCs; □, spd QCs; ●, ■, decagonal phase; ——, locus of ideal NFE; – – –, least-squares fit on the data points, with equation $\bar{k}_{F,NFE} = -0.414 + 1.031\bar{k}_{F,exp}$.

analysis of the variation in relative intensity I of the main diffraction peaks, a linear relation is found between the temperature T_m at which the resistivity minimum is located and the ratio $(I_{211111}+I_{221001})/I_{322101}$. Such a relation strongly supports an NFE model of QCs. Indeed, in the framework of diffraction theory [33] T_{min} is determined by the relative positions of the first peaks of $S(\bar{q})$, $\bar{q}_p$ and $2\bar{k}_F$; the first is temperature dependent and composition independent, while for the others the reverse holds. The origin of the resistivity minimum could be attributed to a shift in $\bar{q}_p$ with respect to $2\bar{k}_F$, on changing temperature, while the shift in the minimum with c could depend on the movement of E_F with respect to the bottom of the DOS pseudogap.

Although transport properties in QCs have been investigated on a still small number of systems, it appears that the stability of QCs, *i.e.* improved quasi-crystallinity, does depend on the electronic structure at E_F, specifically a DOS reduction.

Such mechanism was assessed by isomer shift and quadrupole splitting measurements in AlMnFe alloys which display maxima for the composition $Al_{80}Mn_{11}Fe_9$, indicated as single-phase icosahedral by X-ray diffraction [34]. As a near-neighbour effect when iron is substituted for manganese is ruled out, the quite impressive variations in magnitude and trend of isomer shift have been attributed to changes in the conducting electron distribution, with a meaningful lowering of the electronic DOS at E_F.

TABLE 3

Structure, average valence electron concentration $\langle Z \rangle$ and $\langle Z \rangle$ boundary values for the Hume-Rothery crystalline and non-crystalline phases

Hume-Rothery phase	Structure	$\langle Z \rangle$	Boundary $\langle Z \rangle$
α	F.c.c.	1.00–1.41	1.362
β	B.c.c.	1.35–1.60	1.480
ζ	H.c.p. ($c/a = 1.633$)	1.22–1.83	–
γ	Complex cubic	1.54–1.70	1.620
δ	Complex cubic	1.55–2.00	–
μ	β-Mn	1.40–1.54	–
ϵ	H.c.p. ($c/a = 1.570$)	1.65–1.89	1.700
η	H.c.p. ($c/a = 1.750$)	1.92–2.00	–
QC	Icosahedral	1.45–2.60	–
Amorphous	Disordered	> 1.80	–

Model calculations performed for crystalline approximants of several QCs suggest that the pseudogap at the Fermi level is a universal character of such structures [35], independent of the basic structural units involved in building up three-dimensional Al–TM (Mackay icosahedron) and spd (triacontahedron) QCs.

Table 3 provides a list of Hume-Rothery phases, including crystalline, glassy and quasi-crystalline structures. It is worth noticing that the $\langle Z \rangle$ interval $1.45 \leqslant \langle Z \rangle \leqslant 2.6$ pertinent to the icosahedral phase is comparatively wide. It lies between the $\langle Z \rangle$ values for the highest $\langle Z \rangle$ crystalline phase, namely the η phase, and the lower $\langle Z \rangle$ limit for the amorphous phase.

In conclusion, we believe that the QCs are an electron phase in which energy band effects stabilize an otherwise energetically unfavoured extended packing of tetrahedral structural units.

Acknowledgment

Financial support by Ministero Università e Ricerca Scientifica e Tecnologica is acknowledged.

References

1 P. A. Bancel and P. A. Heiney, *Phys. Rev. B, 33* (1986) 7917.
2 P. A. Bancel, P. A. Heiney, P. W. Stephens, A. I. Goldman and P. M. Horn, *Phys. Rev. Lett., 54* (1985) 2422.
3 U. Mizutani, Y. Sakabe, T. Shibuya, K. Kishi, K. Kimura and S. Takeuchi, *J. Phys. Condens. Matter, 2* (1990) 6169.

4 W. Hume-Rothery, *J. Inst. Met., 35* (1926) 295.
5 H. Jones, *Proc. R. Soc. London, Ser. A, 144* (1934) 225.
6 S. R. Nagel and J. Tauc, *Phys. Rev. Lett., 35* (1975) 380.
7 P. Häussler, F. Baumann, J. Krieg, G. Indlekofer, P. Oelhafen and H.-J. Güntherodt, *Phys. Rev. Lett., 51* (1983) 714.
8 R. Chatterjee and R. C. O'Handley, *Phys. Rev. B, 39* (1989) 8128.
9 D. Bahadur, V. Srinivas, R. A. Dunlap, R. C. O'Handley and M. E. McHenry, *Philos. Mag. B, 60* (1989) 871.
10 A. P. Tsai, A. Inoue and T. Masumoto, *J. Mater, Sci. Lett., 7* (1988) 322.
11 A. Inoue, A. P. Tsai and T. Masumoto, *J. Non-Cryst. Solids, 117–118* (1990) 824.
12 A. L. Mackay, *Acta Crystallogr., 15* (1962) 916.
13 A. Wenzer and S. Steinemann, *Helv. Phys. Acta, 47* (1974) 321.
14 L. Pauling, *Phys. Rev., 54* (1938) 899.
15 G. V. Raynor, *Philos. Mag., 36* (1945) 770.
16 P. Häussler and E. Kay, *Z. Phys. Chem., N.F., 157* (1988) 377.
17 P. M. Ossi, *Radiat. Eff. Defects Solids, 108* (1989) 61.
18 R. Bellisset, F. Bouree-Vigneron and P. Sainfort, *J. Phys. (Paris), Colloq. C3, 47* (1986) 361.
19 H. S. Chen and A. Inoue, *Scr. Metall., 21* (1987) 527.
20 H. S. Chen, J. C. Phillips, P. Villars, A. R. Kortan and A. Inoue, *Phys. Rev. B, 35* (1987) 9326.
21 Y. Sakurai, C. Kokubu, Y. Tanaka, Y. Watanabe, M. Masuda and S. Nanao, *Mater. Sci. Eng., 99* (1988) 423.
22 W. Ohashi, *Ph.D. Dissertation*, University of Harvard, Cambridge, MA, 1989.
23 A. Inoue, K. Nakano, T. Masumoto and H. S. Chen, *Mater. Trans. Jpn. Inst. Met., 30* (1989) 200.
24 Y. Shen, S. J. Poon, W. Dmowski, T. Egami and G. J. Shiflet, *Phys. Rev. Lett., 58* (1987) 1440.
25 M. E. McHenry, V. Srinivas, D. Bahadur, R. C. O'Handley, D. J. Lloyd and R. A. Dunlap, *Phys. Rev. B, 39* (1989) 3611.
26 A. P. Tsai, A. Inoue, Y. Kohohama and T. Masumoto, *Mater, Trans. Jpn. Inst. Met., 31* (1990) 98.
27 P. M. Ossi and D. C. Kothari, *J. Less-Common Met., 171* (1991) 221.
28 J. L. Wagner, K. M. Wong and S. J. Poon, *Phys. Rev. B, 39* (1989) 8091.
29 U. Mizutani, Y. Sakabe and T. Matsuda, *J. Phys.: Condens. Matter, 2* (1990) 6153.
30 D. Bahadur, A. Das, K. Singh and A. K. Majumdar, *J. Phys.: Condens. Matter, 3* (1991) 4125.
31 K. Kimura, H. Iwahashi, T. Hashimoto, S. Takeuchi, V. Mizutani, S. Ohashi and G. Itoh, *J. Phys. Soc. Jpn., 58* (1989) 2472.
32 M. A. Howson and B. L. Gallagher, *Phys. Rep., 170* (1988) 265.
33 H. S. Chen, *Rep. Prog. Phys., 43* (1980) 353.
34 R. D. Werkman, P. J. Schurer, I. Vincze and F. van der Woude, *Hyperfine Interact., 45* (1989) 409.
35 T. Fujiwara and T. Yokokawa, *Phys. Rev. Lett., 66* (1991) 333.